ORIGINAL ARTICLE
Electrica 2026; 26: 1-14

Simulation Analysis and Test Results of Internal Fault Arc Pressure in Medium Voltage Air Insulated Switchgear

Ali Togay[1,2], Gianmatteo Cantoro[3], Hıdır Düzkaya[4], Müslüm Cengiz Taplamacıoğlu[4], Sabri Uzel[1], Engin Göksu[1], Tolga Ünver[5]

[1]R&D Department, Eaton, Ankara, Türkiye
[2]Department of Energy Systems Engineering, Gazi University Graduate School of Natural and Applied Sciences, Ankara, Türkiye
[3]AMS CoE, Eaton, Roztoky-Prague, Czechia
[4]Department of Electrical-Electronic Engineering, Gazi University Faculty of Engineering, Ankara, Türkiye
[5]R&D Department, Eaton, SC, Hengelo, Netherlands

Cite this article as: A. Togay, G. Cantoro, H. Düzkaya, M. C. Taplamacıoğlu, S. Uzel, E. Göksu, T. Ünver. "Simulation analysis and test results of internal fault arc pressure in medium voltage air insulated switchgear," *Electrica*, 26, 0213, 2026. doi: 10.5152/electrica.2026.25213.

WHAT IS ALREADY KNOWN ON THIS TOPIC?

- *Internal arcing significantly influences the fundamental design of medium-voltage air-insulated switchgears, particularly in terms of equipment integrity and personnel safety.*
- *The pressure distribution during the internal arc varies depending on the chamber geometry and the characteristics of the gas discharge structure.*

WHAT THIS STUDY ADDS ON THIS TOPIC?

- *The study examines the time-dependent behavior of the internal arc pressure using CFD and FEA-based calculations and validates the results against experimental test data.*
- *The findings indicate that the flap and chimney structure are critical design parameters for the effectiveness of pressure relief.*

Corresponding author:
Hıdır Düzkaya

E-mail:
hduzkaya@gazi.edu.tr

Received: July 8, 2025
Accepted: September 8, 2025
Publication Date: January 28, 2026

DOI: 10.5152/electrica.2026.25213

ABSTRACT

The occurrence of internal arcing in metal-enclosed medium-voltage switchgear during its service life is rare. However, it remains a critical consideration for ensuring operational reliability and personnel safety. This study investigates the internal arc fault in medium-voltage air-insulated switchgear (AIS) and evaluates the pressure dynamics within switchgear compartments. Computational fluid dynamics (CFD) and finite element analysis (FEA) are performed to simulate and analyze the arc-induced thermal and mechanical effects on the enclosure. The simulations are conducted in accordance with International Electrotechnical Commission 62271-200 standards, considering a rated voltage of 24 kV and short-circuit current of 21 kA for 1 second, validated through internal arc fault tests performed in an accredited laboratory. The CFD results provided insights into pressure and energy distribution, while FEA simulations assessed structural strength under arc-induced stresses. Experimental verification demonstrated a strong correlation with the simulation results, confirming the effectiveness of the proposed modeling approach. The findings of this study contribute to the optimization of AIS design by enhancing safety measures, reducing testing costs, and improving product reliability for medium-voltage switchgear applications.

***Index Terms*—**Air-insulated switchgear, computational fluid dynamics, finite element analysis, internal fault arc, medium voltage

I. INTRODUCTION

Electric power systems constitute the foundation of modern infrastructure, extending across continental scales to supply electricity to homes, offices, factories, and institutions in developed regions while achieving varying levels of reach in developing economies. The electric power grid comprises the entire network of wires and equipment connecting energy sources, such as power plants, to consumers and encompasses both the transmission system, which transmits electricity from power plants to substations, and the distribution infrastructure, which carries electricity from substations to individual users. Commonly, the term "grid" refers specifically to the transmission system, though it is an integral part of the distribution energy within the distribution network [1].

Historically, electricity systems are designed to transport power from large central power plants connected to transmission systems to passive loads in distribution systems; however, in many Organisation for Economic Co-operation and Development countries, new power generation facilities are now integrated directly into distribution systems, which are evolving into active networks with roles in energy import/export and power quality maintenance. While electricity distribution systems exist in public, private, or hybrid forms, they predominantly remain under public administration globally, with notable exceptions in Canada and some South American countries [2].

With advancing technology, power distribution planning (PDP) has gained importance in addressing the growing electricity demand through economical, reliable, and safe methods, incorporating multi-objective optimization techniques such as minimizing investment and operating costs, while leveraging the integration of distributed energy sources like solar and wind, alongside big data and automation systems, to enhance flexibility and reduce energy losses [3].

The distributed system reconfiguration (DSR) problem, originally formulated in 1975, serves as a cornerstone of PDP. Early approaches to DSR relied on classical optimization techniques, which have been effective under limited constraints but struggled with the problem's inherent nonlinearity and high dimensionality. As computational capabilities advanced, heuristic and metaheuristic algorithms such as genetic algorithms and particle swarm optimization have increasingly been applied to DSR, significantly enhancing solution quality and computational efficiency [4, 5].

Parallel to technological advancements, regulatory and economic pressures are shaping investment priorities. The European Union, for example, anticipates that grid-related expenditures will double to support the decarbonization agenda and enable deeper market integration. Rising grid costs, if not carefully managed, could affect energy affordability and economic competitiveness. Regulatory frameworks are thus encouraged not only to focus on cost control but also to support the deployment of innovative infrastructure and technologies that are capable of integrating high shares of renewable energy and electrifying end-use sectors such as transport and heating [2, 6]. With growing demand for resilient, secure, and efficient grids driven by advancements in energy efficiency and the rise of electric transportation, trains, and vehicles, the modernization of technology and processes becomes essential. In contrast, renewable energy remains central to the energy transformation [7]. Electric power systems encompass generation, transmission, and distribution where electricity is generated at optimal voltages, stepped up to extra high voltage (HV) for transmission, reduced to HV for sub-transmission, further lowered to medium voltage (MV) for distribution and finally reduced to low voltage for delivery to domestic or commercial end-users [8, 9]. Between these systems, the 24 kV voltage level is classified as MV according to the International Electrotechnical Commission (IEC) 60038 standard [10] . It is exactly known that the 24 kV voltage level is commonly used in Europe, such as Portugal [11], Spain, the USA, and many Middle Eastern countries such as Saudi Arabia, UAE, and the rest of the GCC countries [12].

In 2023, the global switchgear market has been valued at approximately USD 80.74 billion and is projected to reach USD 87.04 billion in 2024. By 2034, this value is expected to rise significantly, reaching approximately USD 184.46 billion. The market is anticipated to grow at a compound annual growth rate (CAGR) of 7.8% throughout the forecast period from 2024 to 2034. Among several regions, Europe is expected to experience the most rapid expansion in CAGR between 2024 and 2034. Additionally, the switchgear market in the Asia-Pacific region has been valued at approximately USD 39.56 billion in 2023 and is forecasted to reach around USD 90.39 billion by 2034, with a CAGR of 8% over the same period [13]. A metal-enclosed switchgear is a device that is located in different metal compartments of a switchgear used in an electric power system. All these compartments are earthed, and the compartments are separated by metal. It consists of at least three compartments: the breaker, busbar, and feeder. It has mechanical and electrical interlocks that prevent contact with operating personnel with live parts and safety measures that prevent the chance of wrong maneuvers. Switchgear and connection elements used in metal-enclosed cubicles are defined in two main sections air insulated and gas insulated [14, 15]. In this study air insulated switchgear (AIS) is based. In 2024, the global AIS market has been valued at approximately USD 9.9 billion and is projected to expand at a CAGR of 7.8% from 2025 to 2034. This growth is primarily attributed to the increasing demand for reliable and efficient power distribution systems. The AIS technology offers several advantages, including cost-effectiveness, weather resistance, and minimal maintenance requirements, making it a preferred choice in various applications. Leading companies operating in this industry include ABB, Schneider Electric, Eaton, Hitachi, Ormazabal, Siemens, and Lucy Group [16]. The main function of these devices is to safely interrupt the current flow in the event of a fault outside the nominal operating range [17]. All MV devices are designed according to the relevant IEC or IEEE (Institute of Electrical and Electronics Engineers) standards, tested in accordance with the relevant standards in independent international test laboratories, and their approval certificates are made. Among these standards, the IEC 62271 standard specifies general definitions, test methods, and requirements on HV switchgear and control equipment. The IEC 60502 provides information on MV power cables and accessories, and IEC 61230 on earthing and short-circuiting equipment. Similarly, IEEE C37.20 MV switchgear and control equipment, IEEE 400—testing and condition assessment of power cables are standards. Fundamental tests for an AIS product according to IEC standards are: dielectric tests (IEC 62271-1; IEC 60060-1), short time current test (IEC 62271-100; IEC 62271-200), temperature rise test (IEC 62271-1), mechanical strength test (IEC 62271-102), and internal arc test (IEC 62271-200). Upon completion of these tests, the AIS product is designed and tested following the standards. The product mentioned in this article is designed in accordance with IEC standards. As outlined by IEC and IEEE standards, the internal arc classification (IAC) for MV switchgear plays a crucial role in ensuring personal safety during internal arc faults. Over recent years, IAC has become a widely accepted standard for safeguarding individuals. A significant challenge in this context is managing the release of hot gases from the faulty switchgear. The most common approach involves directing these gases through a pressure relief duct that leads outside the switchgear building. Standards such as IEC 62271-200, IEC 62271-202, and IEEE C37.20.7 aim to provide a minimum level of human protection, including for operators and pedestrians. These standards focus on mitigating the hazardous effects of internal arc faults in the vicinity of the switchgear. The internal arc testing procedures described in these standards are designed to assess the system's ability to protect individuals under the worst-case scenario of an internal arc, taking into account factors such as overpressure, thermal impacts, and the release of hot gases [18]. The design of MV switchgear must prioritize the highest level of safety for operating personnel and be capable of confining the effects of an arc fault to the specific compartment where it occurs. While internal arc faults are rare in modern switchgear, their occurrence can significantly damage equipment and buildings and even pose serious risks to human life [19]. Internal arc testing for metal-enclosed MV switchgear, mandated by IEC standards that prohibit confirming internal arc withstand capability through calculations, is widely practiced ensuring protection for individuals due to the higher accessibility of MV systems compared to high-voltage installations [20, 21]. In this study, the rated voltage level for AIS is focused on 24 kV, and

literature studies related to 24 kV are examined. Rochette et al. developed a mathematical model and numerical method to simulate the mechanical and thermal phenomena in a porous filter-like energy absorber during a 24 kV GIS medium-voltage internal arc fault [22]. Teera-Achariyakul and Hokierti evaluated internal arc pressure in a GIS medium-voltage outdoor compact substation by analyzing arc voltage drop and arc energy, determining that a portion of this energy vaporizes busbar and compartment metal, contributing to high internal pressure, which is assessed through pressure analysis of the evaporated metal [23].

The product design is shaped with the arc and pressure values obtained with the computational fluid dynamics (CFD) analyses made by taking the length and duration of the electric arc as a reference and the FEA analyses made by taking the CFD analysis results as a reference for an AIS MV product designed in line with market needs at 24 kV 21 kArms and 25 kArms in 1 second. It is observed experimentally in DEKRA laboratories following the IEC 62271-200 standard, and successful results have been obtained. The successful results obtained will provide a highly accurate idea before performing the test verification for developing new products to solve the increasing market needs with the developing technology. In this way, serious savings will be provided not only in terms of test product preparation and test costs but also in terms of time.

II. MATERIAL AND METHODS

This study integrates methodologies and results from various studies to develop a comprehensive understanding of internal arc faults in MV switchgear systems, supporting CFD and FEA analyses and validating with IEC 62271-200 internal arc type test results.

A. Simulation Methods

The AIS products are designed in 3D in the SolidWorks environment and then transferred to the ANSYS environment to start the analysis processes. Although they are done on the same program, the CFD and FEA processes have fundamental differences in terms of progress. As shown in Fig. 1, the AIS product designed is transferred to the ANSYS environment with the "imported model." Since the mechanical properties of the material exposed to pressure are of great importance for FEA analyses, material selections are made before the mesh step. In the CFD model, determining the energy equations to be applied ensures the correct solution of each mesh structure. Then, the analysis process is completed with each mesh solution by determining the boundary conditions.

1) Computational Fluid Dynamics Analysis Method and Model:

During the internal arc formation, the arc energy is transferred to the environment through conduction, convection, and radiation. Some energy is transferred to heat, melt, and evaporate the components in the internal arc environment. The remaining energy shows its physical effect in the internal arc environment, such as temperature and pressure. This physical process can be analyzed by mathematical modeling and numerical calculations. However, these calculations are quite complicated due to the complex geometry of the product in which the internal arc is made. The CFD creates partial differential equations based on the mass transfer, momentum transfer, and energy transfer laws of fluid mechanics, and it solves these equations numerically using the finite element analysis (FEA) method. ANSYS Fluent CFD software is used for the modeling.

The governing hydrodynamic equations for conserving mass, momentum, and energy are employed to analyze the temperature distribution and gas flow dynamics within the arcing plasma. These equations are solved through the Navier-Stokes framework, formulated as a generalized transport Equation (1) is given below where, ϕ represents the conserved variables under consideration, ρ is the gas density, v is the gas velocity, Γ is the transport coefficient of ϕ, and S is the source term for ϕ [19, 24]. In addition, the analysis program has calculated the arc energy with the power system formulas by taking

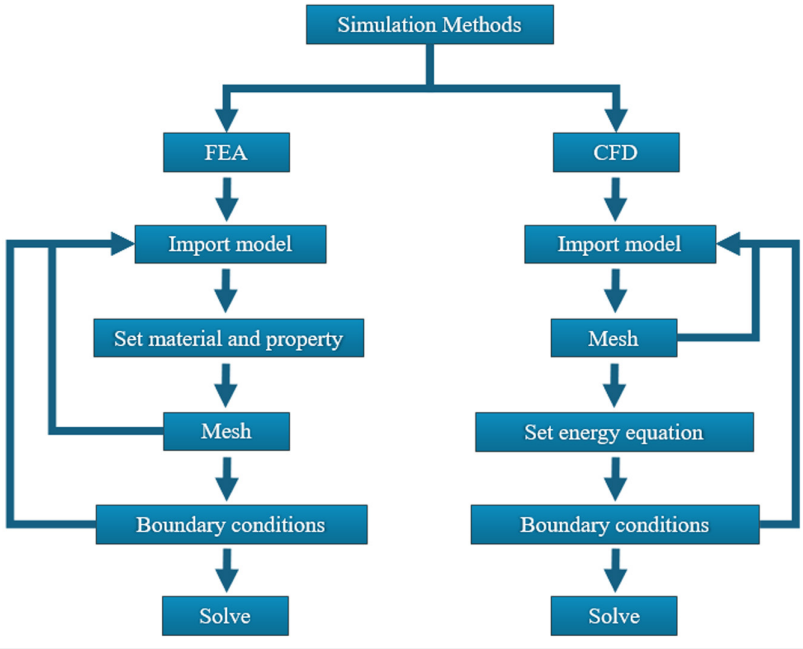

Fig. 1. Algorithm of CFD and FEA.

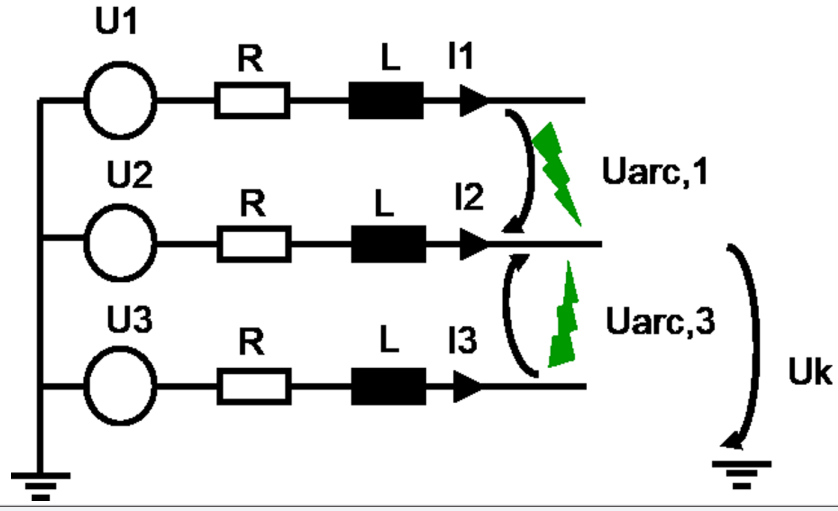

Fig. 2. Internal arc ignition simulation.

into account the phase angle and instantaneous voltage expressions in AC circuits with the Equations (2–5).

$$\frac{\partial}{\partial t}(\rho\phi)+\nabla(\rho v\phi)=\nabla(\Gamma\nabla\phi)+S \quad (1)$$

$$L\frac{dI}{dt}+RI+U_{arc}=U_o \quad (2)$$

$$U_o=\sqrt{2}V\sin(\omega t+\alpha) \quad (3)$$

$$R=\cos\phi\frac{V}{I} \quad (4)$$

$$L=\frac{\sin\phi}{\omega}\frac{v}{I} \quad (5)$$

This experimental simulation is designed to investigate the internal arc formation in HV electrical systems and to evaluate the safety performance of the system. In the circuit, voltage sources (U_1, U_2, U_3) are the basic components that trigger the internal arc formation by operating at different potential levels as shown in Fig. 2. While resistances (R) provide control of voltage drops by limiting the current flow in the system, inductances (L) determine the dynamic response of the circuit and reflect the inductive response of the system to current changes. $U_{arc,1}$ and $U_{arc,3}$ give the internal arc voltage changes in the circuit resulting from the electrical fault.

Fig. 3 presents the different components retained for the CAD model of the MV metal-enclosed AIS panel to be subject to internal arc testing. In accordance with IEC 62271-200, the internal arc test should be performed independently in the cable and the busbar compartments by generating an arc in the relevant compartment.

The internal arc areas are detailed in Fig. 4. While arc ignition on top of the busbar compartment is shown in Zone 1 in Fig. 4 (a), arcing simulation inside the cable compartment is given in Zone 3 in Fig. 4 (a). Additionally, flaps open between the inside volume and chimney with gradually increasing pressure, as shown in Zone 8 in Fig. 4 (b). These flaps not only separate the chimney section from the cable section as in Fig. 4 (a)–2, but also support exhausting the pressure by opening after the internal arc.

2) Finite Element Analysis Method and Structural Model

Finite element analysis is used in various fields, including structural (static and dynamic loads), thermal analysis, fluid dynamics, electromagnetic analysis, and biomechanical applications. This method provides a practical approach for situations where analytical solutions are not possible or practical, allowing for a deeper understanding of engineering problems. However, the accuracy of the analysis depends on the appropriate definition of mesh quality, material

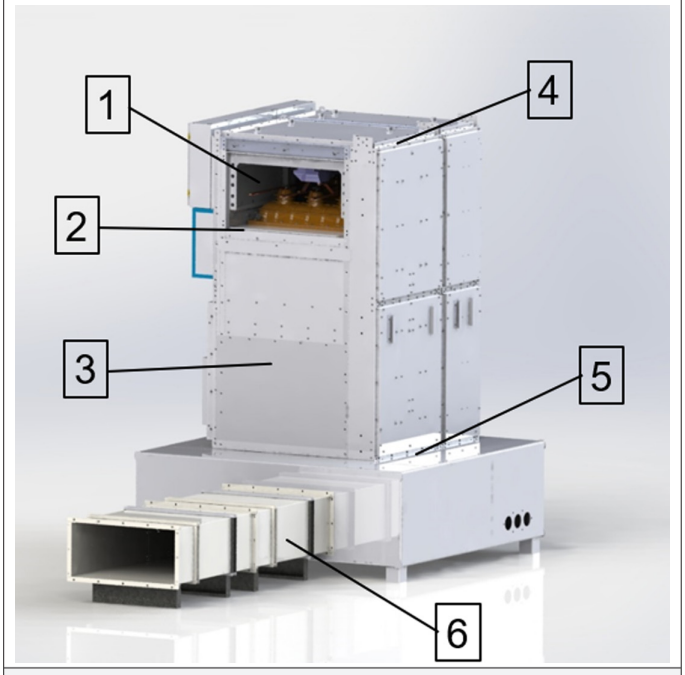

Fig. 3. Description of the CAD model: (1) busbar compartment, (2) busbar and cable compartments separation surface, (3) cable compartment, (4) top chimney, (5) bottom chimney and (6) exhaust duct.

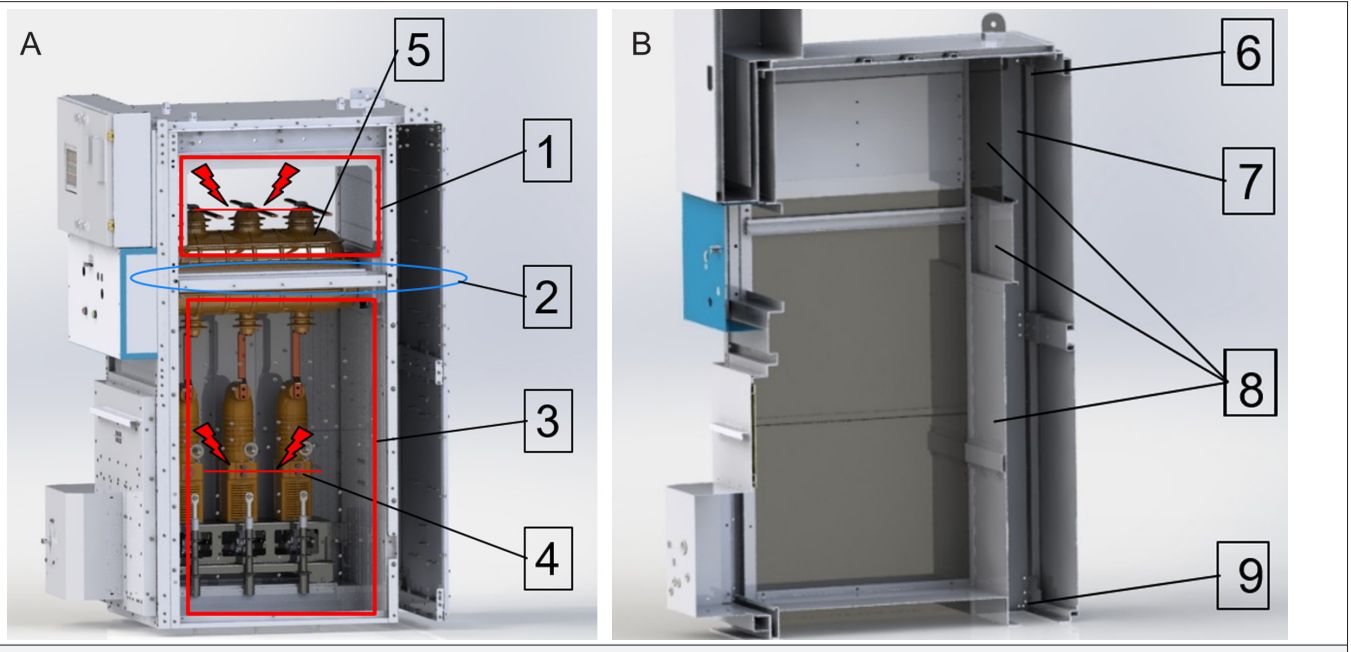

Fig. 4. Internal arc areas: (a) compartment zones: (1) busbar zone, (2) busbar and cable compartment separator surface, (3) cable compartment zone, (4) vacuum circuit breaker (VCB), (5) disconnector switch; and (b) chimney zones: (6) top chimney, (7) chimney area, (8) flap zones, (9) bottom chimney.

models, and boundary conditions. The basic principle of analysis is to divide a continuous structure into small, discrete elements and mathematically express the behavior of each element. This approach is used to obtain an approximate solution of partial differential equations. ANSYS software is used for the modelling.

The length of the arc duration, depending on the time the arc remains in the relevant compartments, determines the amount of energy that is transferred to the gas. The pressure field is obtained from this amount of energy depending on the duration. The pressure outlet boundary condition is assigned to the walls open to the atmosphere. The gas pressure in the compartment affects the inner metal surfaces of the AIS product, causing elastic and plastic deformations. The mesh size is chosen such that the effect of pressure on the product is precisely described by the model. Nonlinear material properties have been considered for the metal enclosed. 837729 nodes and 807292 elements are used in this model.

B. Test Setup

Tests are performed according to IEC 62271-200 standards defining internal arc fault classification and personal safety criteria. The internal arc test is performed according to IEC 62271-200 AFLR requirements at 24 kV, 21 kA rms, and 25 kA rms for 1 second. Cotton cloth indicators are placed in Fig. 5 (a) to evaluate the pressure and temperature effects caused by the AFLR internal arc. The indicators are placed across a metal platform and fixed in all accessible places on

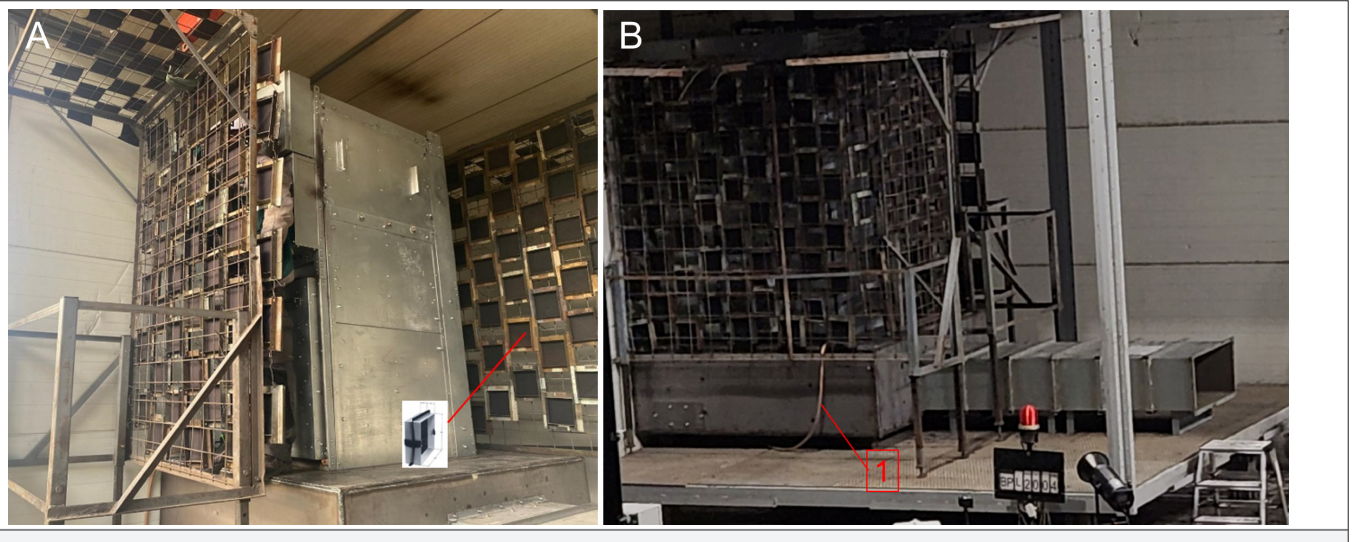

Fig. 5. Test setup view.

the product. The cloth simulates the clothing of people working in close proximity to the product [19]. According to the IEC 62271-200, standard five criteria must be performed for the test to be completed,

- Secured doors and covers do not open.
- Scattering small items with an individual mass of up to 60 g is acceptable.
- Arcing does not cause holes in the accessible areas up to the height of 2 m.
- Cotton indicators shall not ignite from hot gases or arc effects.
- Fig. 5 (b)–1 The primary earth connection should not be separated from the central unit because of internal arcing.

The most important of these indicators is that they are not ignited by hot gases or arc ignition [18, 20].

Cotton cloth indicators evaluate the thermal effects of hot gases released from the installation due to pressure build-up caused by an arc fault. These indicators are placed on a rack configured in a checkerboard pattern on the accessible side(s) of the switchgear. The fabric simulates the clothing of individuals near the installation. The most crucial criterion for passing internal arc tests is the absence of damage to these indicators [21]. An internal arc is triggered within the switchgear panel using a thin wire, shortening the phases during these tests. Cotton cloth indicators, which simulate human clothing and are positioned near accessible areas, must not catch fire due to the internal arc by-products [15].

III. RESULTS AND DISCUSSION

All results are organized under two headings: simulation results and test results. Since the internal arc tests are tested independently of each other as the cable compartment and busbar compartment, the pressure variation in each compartment is examined separately.

A. Simulation Results

1) CFD Results:

The changes in the electric arc power (blue curve) and arc energy (red curve) are shown in Fig. 6 during the first 500 ms. The arc power increased instantly at the beginning and reached around 65 MW. This situation shows that the arc requires high energy at ignition. Afterward, it passes into a wavy structure, and since the network frequency is 50 Hz, it is seen that it makes a minimum at the values of 10-20-30-40 to 100 ms, which are the zero crossing points for 50 Hz, and then makes local maximums in the 90°–270° regions.

The arc energy is a cumulative total of the arc power depending on time and reaches approximately 17500 kJ at the end of 500 ms. While the power value fluctuates, the energy accumulation continues to increase continuously. This shows that the arc is constantly accumulating energy. This accumulated energy is transferred to the materials as heat and to the air as heat and pressure affect the internal environment.

In this study, particular emphasis is placed on 24 kV AIS configurations. The product evaluated is designed and validated under IEC 62271-200 standards, with arc ratings of 21 kArms and 25 kArms for 1 second. Coupling CFD and FEA simulations has allowed for the precise tuning of internal pressure management systems, resulting in substantial savings in both development cost and testing time. These findings highlight the value of simulation-driven design in meeting the growing demand for resilient and efficient MV switchgear tailored to the evolving requirements of smart and sustainable energy networks.

Fig. 7 shows the change in the over-pressure value resulting from the internal arc in the busbar compartment in the first 80 ms, not only in the busbar compartment but also in the top chimney and bottom chimney. At 22 ms, the pressure in the top and bottom chimney starts rising. It corresponds to the time the flaps open because the average pressure at the surface of the flap reaches a relative 1.5 bar, letting the pressurized gas enter the top and bottom chimney. It is observed that the pressure fluctuation periods in the top and bottom chimneys have 10 ms half-wave periods, as in Fig. 6. This situation shows that the impacts originating from the 10 ms periods of the arc power in Fig. 7 directly affect the top and bottom chimneys as pressure after the flaps open. The pressure peaks at the top and bottom of the chimney at 25 ms are the same at 0.5 bar, as shown in Fig. 7. The pressure value tends to decrease between 25 and 30 ms;

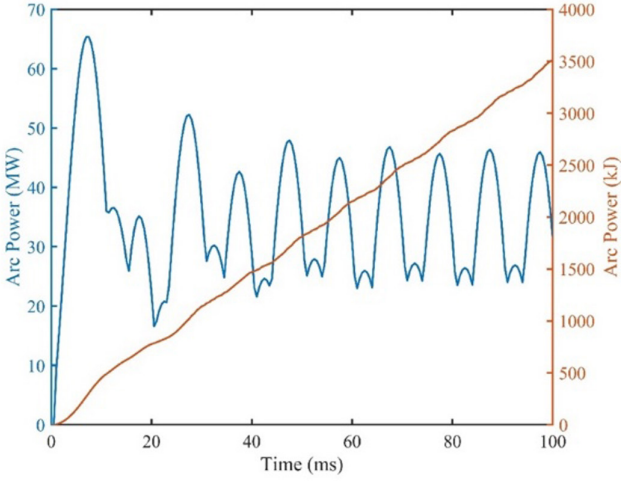

Fig. 6. Arc energy and power variation versus time.

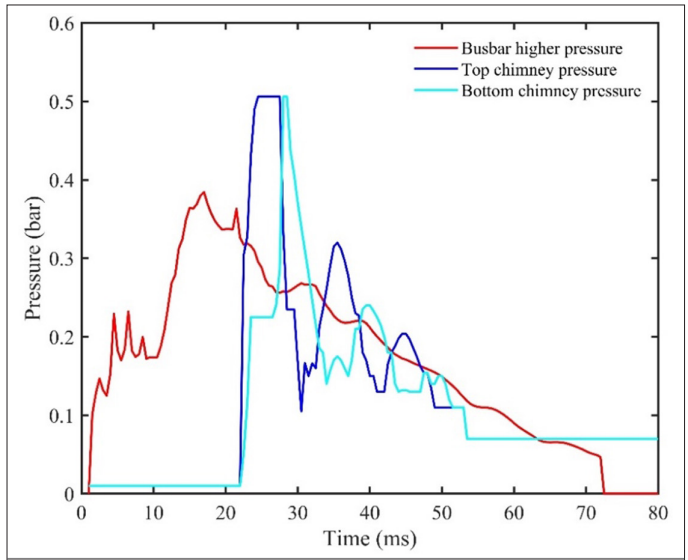

Fig. 7. Overpressure in the busbar compartment and chimney zone.

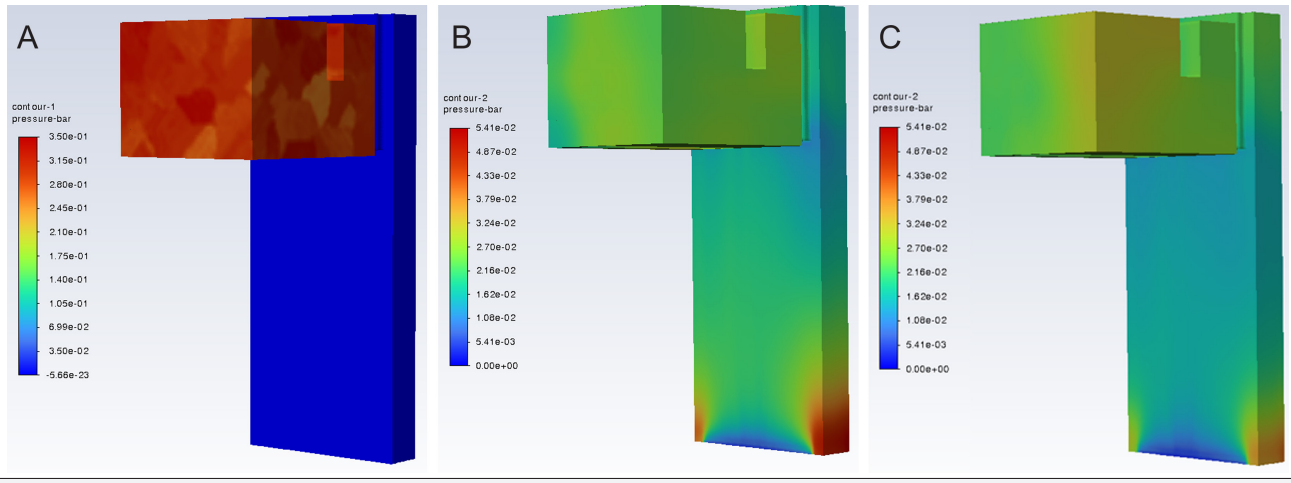

Fig. 8. Pressure behaves at different times (a) 16 ms, (b) 40 ms, and (c) 50 ms.

however, after 30 ms, partial pressure increases are observed at the top and bottom of the chimney. This is owing to the waste gas generating an offset due to the back pressure before being evacuated. This situation is related to the geometry of the chimney and the flaps. The pressure distribution in the busbar compartment varies depending on factors such as the timing of the flap opening, the flap geometry, and the volume of the chimney chamber [25, 26]. The faster the flaps open and the faster the exhaust gas is evacuated, the more stable the graph is going to be.

Fig. 8 shows pressure field at different times. As shown in Fig. 8 (a) the situation in the first 16 ms after the ignition in the busbar compartment, the flaps have not opened yet, and the pressure is gradually increasing. Fig. 8 (b) shows pressure field at 40 ms. Even though the pressure effect is still observed in the busbar compartment, the pressure value is higher in the bottom chimney than in the busbar compartment. Fig. 8 (c) also simulates the behavior at 50 ms. The pressure values in the busbar compartment and the pressure values in the bottom chimney are almost the same. However, since the waste gas is exhausted from the bottom chimney, the duration of exposure to pressure is longer than that of the busbar compartment, and pressure effects are observed further at the bottom of the chimney.

Dullni et al. [27] demonstrated that the fault current had a value of 35 kA and was applied at the busbar compartment for 1 second. As a result of their experiment, the pressure value reached up to 2.5 bar. Kumar et al. [19] claim that the pressure change in different areas of the busbar compartment is 0.4–2.1 bar. When the results are compared to the findings, the pressure value obtained from the design was lower than the value of the findings of Dullni et al. [27] but almost the same as the results of Kumar et al. [19].

Fig. 9 shows the change in the pressure value resulting from the internal arc in the cable compartment in the first 80 ms, not only in the cable compartment but also in the top chimney and bottom chimney. It is observed that the pressure fluctuation periods in the top and bottom chimneys have 10 ms half-wave periods, as in Fig. 6. This situation shows that the impacts originating from the 10 ms periods of the arc power in Fig. 6 directly affect the top and bottom chimneys as pressure after the flaps open. As seen in Fig. 9, the peak value at the top of the chimney is higher than the cable compartment section at 25 ms. While the pressure value tends to decrease at 30 ms, partial pressure increases are observed at the top and bottom of the chimney after 32 ms. This is because the exhaust gas creates an offset due to back pressure before being evacuated. This situation is completely related to the geometry of the chimney and the flaps. The pressure distribution in the cable compartment varies depending on factors such as the timing of the opening of the flaps, the flaps geometry, and the volume of the chimney chamber. The faster the flaps open and the faster the exhaust gas is discharged, the more stable the graph is. Since the gas in the cable section first goes up to the upper chimney and then goes out through the exhaust, the gas circulates inside for a longer time than in the busbar compartment.

As shown in Fig. 10 (a), the situation is in the first 20 ms after the ignition in the cable compartment. The flaps have not opened yet, and the pressure is gradually increasing. Fig. 10 (b) simulates the behavior of the pressure at 35 ms. The effect of the pressure is still observed in the cable compartment. However, the highest pressure value is at the top chimney at 25 ms and is approximately 3.5 times that of

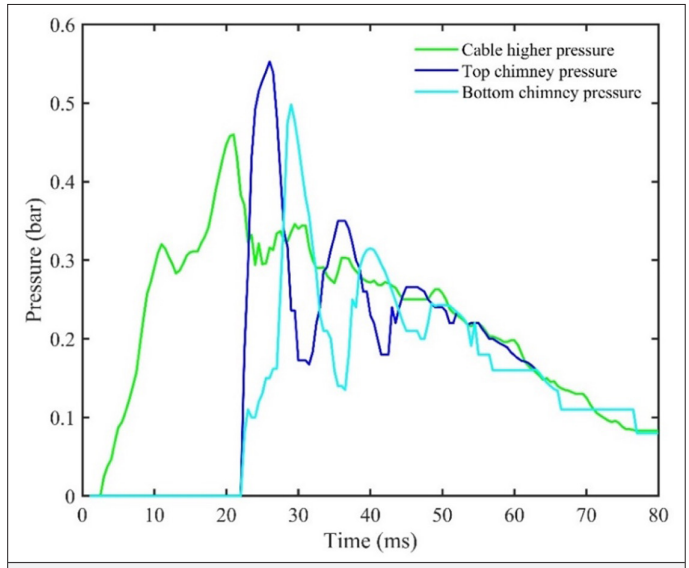

Fig. 9. Change of pressure in the cable compartment and chimney zone.

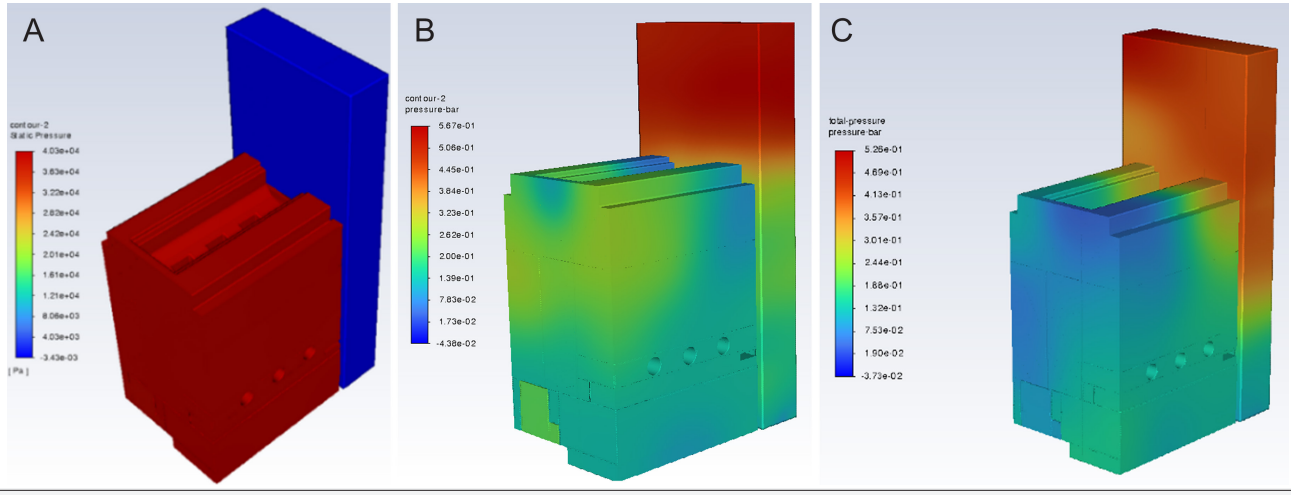

Fig. 10. Pressure behaves at different times (a) 20 ms, (b) 35 ms, and (c) 45 ms.

the bottom chimney. Fig. 10 (c) also simulates the behavior at 45 ms. There is almost considerable pressure left in the cable compartment. Although the top chimney region has the highest pressure value at 35 ms, the pressure effect has decreased due to the exhaust, which has approximately twice the pressure of the bottom chimney.

As shown in Fig. 7 and Fig. 9, the pressure changes in the busbar and cable compartments occurred in different periods. Since the volume of the busbar section is smaller than the cable section, the busbar section reached the highest pressure value in a shorter time. As seen in Fig. 8 and Fig. 10, the high-pressure fluctuations in the upper and lower chimneys correspond to a period of 5 ms, whereas the arc power has a half-wave period of 10 ms. In addition to the back pressure effect, the opening direction of the flaps also affects the pressure fluctuation.

Singh et al. [24] displayed a strong correlation between the simulated and experimental pressure rise values. Pressure measurements are also conducted in the rear duct during their internal tests. The pressure values are achieved at approximately 0.5 bar. El Ouadhane et al. [18] have shown clearly that the initial pressure measurements observed between 0.4 and 2 bar are subsequently reduced by all components of the designed pressure relief system. Kumar et al. (2018) declare that the pressure change in different areas of the cable compartment is 1.1–1.25 bar. Matin et al.'s CFD dataset, which they developed using real switchgear geometry and operating conditions, consists of 54 simulation examples [28]. In addition, the measurement devices show a variation in maximum pressure values throughout the dataset, ranging from 0.18 bar to 1.4 bar. Detailed results of the literature are summarized in Table I.

When the cable compartment data acquired are compared to the literature, it is observed that the results are close to each other except for the peak values. The peak values are different because the short-circuit currents are different, and the power value is directly proportional to the square of the short-circuit current.

2) Structural Results:

A transient structural analysis of all chambers within the MV panel is independently performed utilizing pressure data derived from CFD simulations. This study focuses exclusively on the side walls, rear unit, and doors exhibiting significant stress levels and deformations under specific internal arc fault conditions. The material elongation is 18%, and strains higher than 14% indicate a possibility of cracks being developed in the local regions. The parts are mainly below the yield limit, and those above yield can be processed by

TABLE I. REPORTED EXPERIMENTAL INTERNAL ARC PRESSURE RISE FOR MV AIS PRODUCTS IN THE LITERATURE

References	Number of Phases	Short-Circuit Current	Internal Arc Area	Pressure Rate (bar)
Dullni et al.	3	35 kA 1 s	Busbar compartment	2.5
Kumar et al.	3	40 kA 1 s	Busbar compartment	0.4–2
Present work	3	21 kA 1 s	Busbar compartment	0.5
Kumar et al.	3	40 kA 1 s	Cable compartment	1.1–1.25
El Ouadhane et al.	3	40 kA 1 s	Cable compartment	0.4-2
Singh et al.	3	NA	Cable compartment	0.5
Matin et al.	3	31.5 kA 1 s	Cable compartment	0.17–1.4
Present work	3	21 kA 1 s	Cable compartment	0.5-0.7

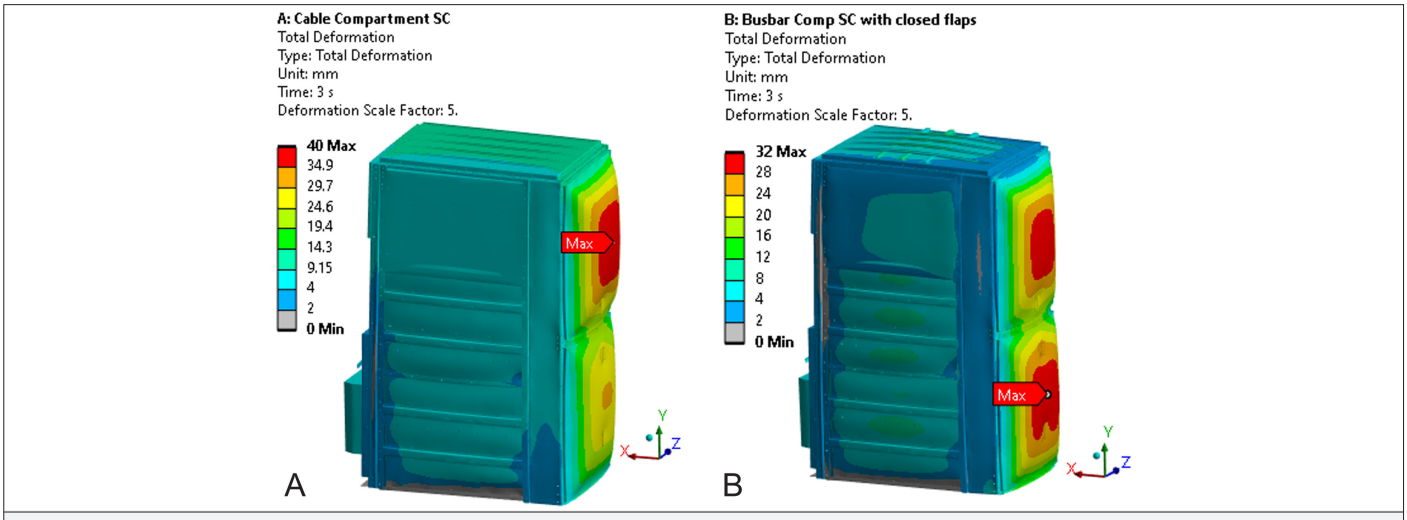

Fig. 11. Total deformation of back cover (a) cable compartment SC, and (b) busbar compartment SC with closed flaps.

the Neuberization method. The Neuberization technique estimates the peak strain experienced by copper microvias. This approach is based on Neuber's rule, which states that a stress concentration factor can determine localized stress and strain. This factor equates the strain energy of an elastic-plastic material to that of an equivalent elastic material, enabling a more accurate estimation of local deformations [28]. Neuber's rule can be fundamentally understood as the principle that the product of stress and strain remains equivalent in both the pseudo-elastic case, where stress and strain are treated as variables, and the elastoplastic case, where these variables account for plastic deformation effects [29]. In 1961, Neuber introduced a method for estimating stress in concentration regions, based on stress analysis of prismatic bodies subjected to shear stress. This approach defines the relationship between stress and strain in purely elastic conditions and those observed in arbitrary elastoplastic behavior [30]. Bolt and rivet joints are observed to be safe for the loads.

Structural analysis studies are divided into two cable and busbar sections. Within the scope of the analysis in the cable section, it occurred for side walls, front unit, rear unit, and back cover. Within the scope of the analysis in the busbar section, it occurs for busbar covers, top unit, and back cover. For the back cover, the internal arc conditions of both the cable and busbar sections are considered separately. In the busbar compartment analysis, side walls and front and rear unit changes are not considered since they will be minimal.

Maximum deformation is observed on the rear panels of the chimney area for both loading cases prominently in the –x direction. The maximum deformation observed in the cable compartment short-circuit scenario is 40 mm. The maximum deformation observed in the busbar compartment short-circuit scenario is 32 mm (Fig. 11). It has been concluded that these deformation values are acceptable as they do not cause gas leakage to the external environment after the applied pressure and deformation that would invalidate the

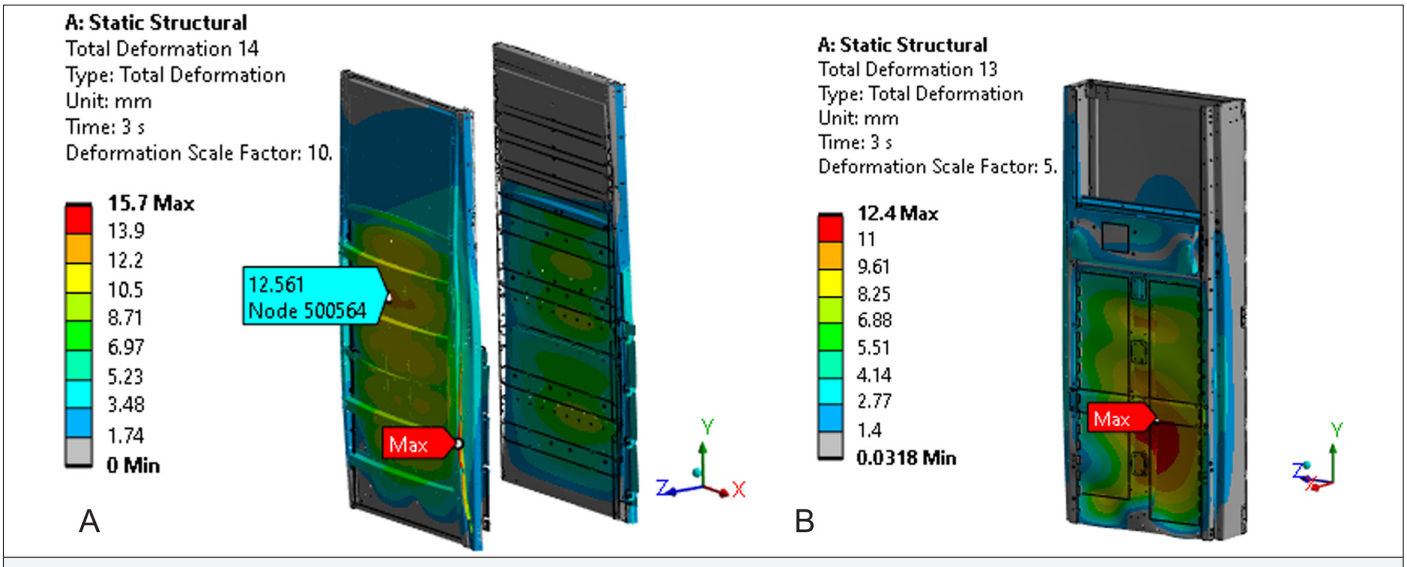

Fig. 12. Total deformation of (a) side walls and (b) rear unit.

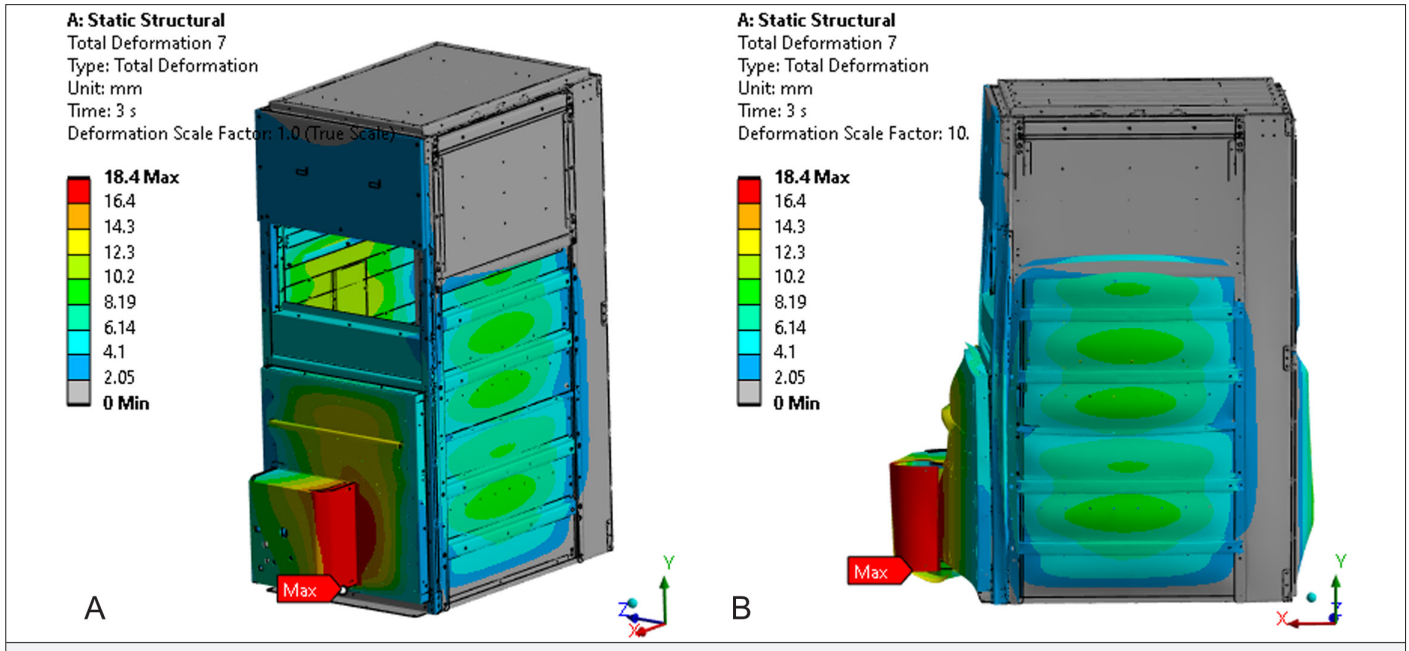

Fig. 13. Total deformation of the front unit with a different view.

test. Figures are shown at a scale of 5 times larger than the actual deformation.

The total deformation of the side unit is around 12.5 mm, and of the rear unit is around 12 mm in Fig. 12. It has been concluded that these deformation values are acceptable as they do not cause gas leakage to the external environment after the applied pressure and deformation that would invalidate the test. Gray lines show undeformed wireframe. Figures are shown at 10 times larger scaled the actual deformation.

The total deformation of the AIS assembly is around 18.40 mm in the front unit, but the design showed no gap between the door and the front panel, as seen in Fig. 13. It has been concluded that these deformation values are acceptable as they do not cause gas leakage to the external environment after the applied pressure and deformation that would. The total deformation of the busbar side cover is around 12.83 mm, as shown in Fig. 14. It has been concluded that these deformation values are acceptable as they do not cause gas leakage to the external environment after the applied pressure and deformation, which would not invalidate the test. Figures are shown at 10 times larger scaled the actual deformation.

As seen in Table II, the deformation rates of the cable compartment areas are higher than the busbar section. This is due to the more significant pressure changes in the cable compartment. Although the surface area of the side covers in the busbar compartment is smaller than the surface area value of the side walls in the cable compartment, the deformation rates are close. This is owing to the similar reinforcement structures among the two sections.

B. Test Results

All cable and busbar internal arc tests are carried out separately in the DEKRA laboratory, and all tests are completed successfully.

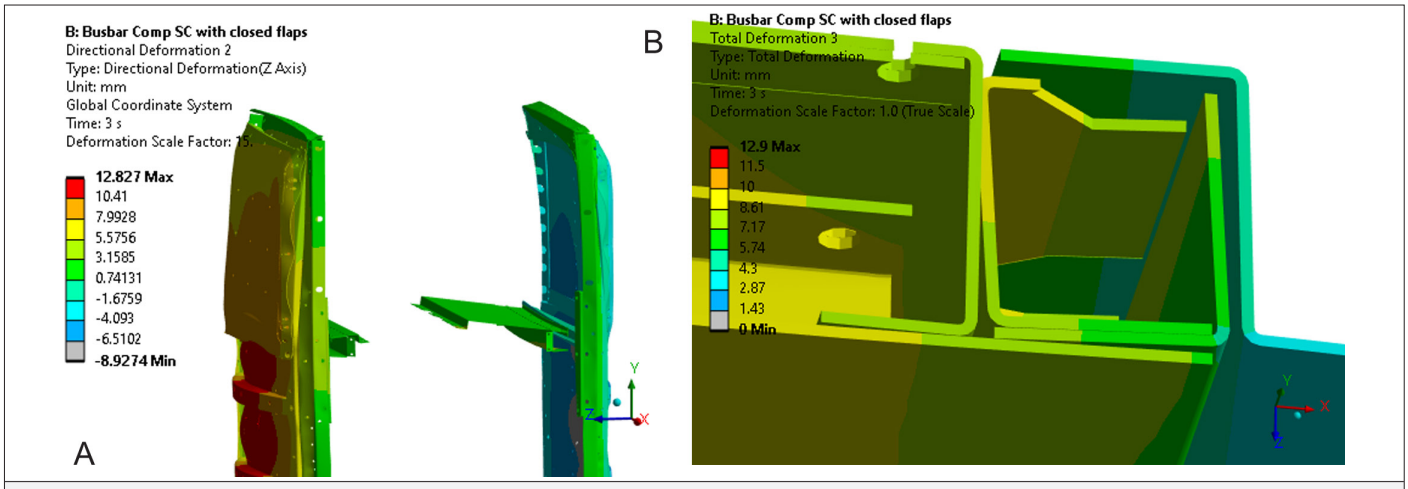

Fig. 14. Total deformation of busbar side cover.

TABLE II. THE RESULTS OF DEFORMATION RATE FEA VALUES

Area		Unit	Deformation Rate
Cable compartment	Side walls	mm	15.7
	Front		18.4
	Rear unit		12.4
	Back cover		40.0
Busbar compartment	Back cover	mm	32.0
	Side cover		12.8

TABLE III. THE RESULTS OF DEFORMATION RATE TEST OBJECTS

Area		Unit	Deformation Rate
Cable compartment	Side walls	mm	0.8
	Front		0
	Rear unit		1.2
	Back cover		5.0
Busbar compartment	Back cover	mm	4.0
	Side cover		4.3

Similar results are obtained when the test data is compared with the CFD data. No measurable deformation is observed when the post-test FEA data are compared with the test products. Thus, better results are obtained than the FEA data. Fig. 15 (a) and (b) show the changes after the test on the front surface. Fig. 15 (c) and (d) show the changes after the test on the side surfaces. No measurable deformation is observed.

After the internal arc test, measurements of the relevant sections are made on the test products. The results obtained are listed in Table III. When compared to the FEA results, very low values are obtained. The main reasons for this may be the overly safe selection of the safety factor in the FEA analysis, the inability to model the evacuate of the waste gas as close to reality, and the less attention paid to the absorbed part of the energy released after the internal arc, such as heat, light and carbonization.

IV. CONCLUSIONS

This study provides a comprehensive analysis of internal arc faults in medium-voltage AIS, emphasizing the pressure dynamics within different compartments. By integrating CFD and FEA, the research successfully models and evaluates the effects of arc-induced thermal and mechanical stresses, ensuring compliance with IEC 62271-200 standards. The CFD simulations effectively captured the evolution of arc energy and pressure distribution, revealing significant fluctuations that impact structural integrity. These findings are validated through experimental testing in accredited laboratories, demonstrating a strong correlation between simulated and observed data. The FEA results further confirmed that the deformation levels remained within acceptable safety limits, ensuring the containment of arc-induced pressure without structural failure or risk to personnel. One of the key insights gained from this study is the critical role of product geometry and flap design in mitigating the effects of internal arc faults. The results indicate that the shape, size, and placement of flaps directly influence pressure distribution and exhaust efficiency. Properly designed flaps allow for rapid pressure relief, minimizing fluctuations, and preventing excessive mechanical stress on the switchgear enclosure. Additionally, the overall geometry of the switchgear plays a fundamental role in controlling the internal flow of hot gases, ensuring that pressure is effectively managed without compromising structural integrity. A key outcome of this study is the validation of a simulation-driven approach to AIS design, which enhances safety measures while reducing the need for extensive physical testing. The findings contribute to the advancement of AIS technology by offering a robust methodology for internal arc fault assessment, ultimately enhancing the reliability and safety of medium-voltage switchgear in industrial applications. Future work

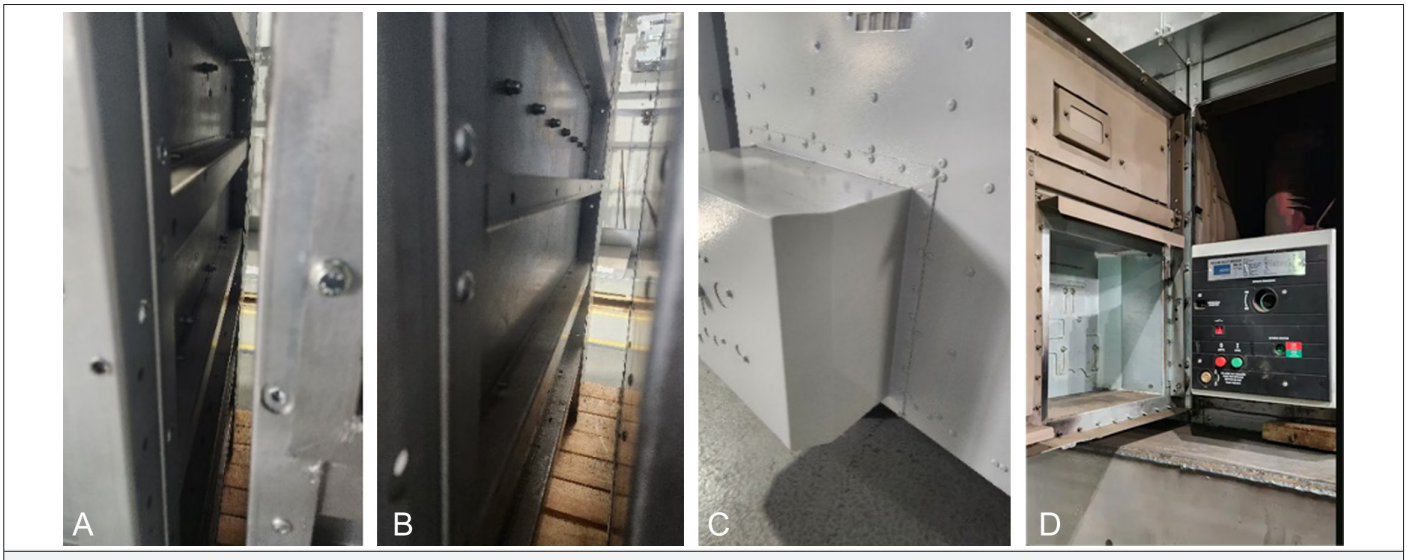

Fig. 15. Deformation observation after internal arc.

may focus on the development process for new AIS products that can be optimized, leading to significant cost and time savings.

Data Availability Statement: The data that support the findings of this study are available on request from the corresponding author.

Peer-review: Externally peer-reviewed.

Author Contributions: Concept – A.T., H.D., S.U.; Design – A.T., S.U., E.G.; Supervision – H.D., M.C.T., T.Ü.; Resources – G.C., E.G., S.U.; Materials – A.T., G.C., T.Ü.; Data Collection and/or Processing – A.T., G.C., S.U.; Analysis and/or Interpretation – A.T., G.C., E.G.; Literature Search – A.T., H.D., E.G.; Writing – A.T., H.D., M.C.T.; Critical Review – H.D., M.C.T., T.Ü.

Declaration of Interests: The authors have no conflicts of interest to declare.

Funding: The authors declared that this study has received no financial support.

REFERENCES

1. M. Amin, and J. Stringer, "The electric power grid: Today and tomorrow," *MRS Bull.*, vol. 33, no. 4, pp. 399–407, 2008. [CrossRef]
2. S. Kufeoglu, M. Pollitt, and K. Anaya, *Electric Power Distribution in the World: Today and Tomorrow*. Cambridge: University of Cambridge, 2018, pp. 1–29.
3. P. S. Georgilakis, and N. D. Hatziargyriou, "A review of power distribution planning in the modern power systems era: Models, methods and future research," *Electr. Power Syst. Res.*, vol. 121, pp. 89–100, 2015. [CrossRef]
4. M. Mahdavi, H. H. Alhelou, N. D. Hatziargyriou, and F. Jurado, "Reconfiguration of electric power distribution systems: Comprehensive review and classification," *IEEE Access*, vol. 9, pp. 118502–118527, 2021. [CrossRef]
5. A. R. Jordehi, "Optimisation of electric distribution systems: A review," *Renew. Sustain. Energy Rev.*, vol. 51, pp. 1088–1100, 2015. [CrossRef]
6. ACER, "Electricity infrastructure development to support A competitive and sustainable energy system," 2024. [Online]. Available: https://www.acer.europa.eu/sites/default/files/documents/Publications/ACER_2024_Monitoring_Electricity_Infrastructure.pdf.
7. M. I. Henderson, D. Novosel, and M. L. Crow, *Electric Power Grid Modernization Trends, Challenges, and Opportunities*. New York: IEEE, 2017, pp. 1–17.
8. B. M. Weedy, B. J. Cory, N. Jenkins, J. B. Ekanayake, and G. Strbac, *Electric Power Systems*, 5th ed. Chichester, UK: John Wiley & Sons, 2012.
9. A. A. Sallam, and O. P. Malik, *Electric Distribution Systems*, 2nd ed. Chichester, UK: John Wiley & Sons, 2018.
10. IEC 60038 "IEC 60038:2009 – Standard Voltages, International Electrotechnical Commission, Geneva", 2009.
11. S. M. Pinto, J. R. Gouveia, J. Atilano, R. C. Gonçalves, L. Tovar, P. C. Lima and L. Oliveira, "Cradle-to-gate life cycle assessment comparison between two switchgear designs: Eliminating SF6 gas under European legislation," *Environ. Impact Assess. Rev.*, vol. 112, p. 107791, 2025. [CrossRef]
12. MarketsandMarkets, "Air insulated switchgear market by installation (Indoor, Outdoor), voltage (Low, Medium, High), application (Transmission & Distribution Utilities, Industrial, Commercial & Residential, Transportation) and region - Global forecast to 2029," 2024. [Online]. Available: https://www.marketsandmarkets.com/Market-Reports/air-insulated-switchgear-market-79980057.html.
13. Precedence research, "*Switchgear Market Size to Hit USD 184.46 billion by 2034*". 2024. [Online]. Available: https://www.precedenceresearch.com/switchgear-market.
14. C. Yundong, L. Xiaoming, W. Erzhi, L. Changxie, and L. Hongfeng, "Investigation on insulation performance for medium voltage vacuum switch cabinet," in IEEE: Proc. of the 21th Int. Symposium on Discharges and Electrical Insulation in Vacuum, 2004, pp. 660–663. [CrossRef]
15. R. Smeets, L. Van der Sluis, M. Kapetanovic, D. F. Peelo, and A. Janssen, *Switching in Electrical Transmission and Distribution Systems*. Chichester, UK: John Wiley & Sons, 2015.
16. Global market insights, "Air insulated switchgear market size - By voltage, by application analysis, growth forecast, 2025–2034," 2025. [Online] Available: https://www.gminsights.com/industry-analysis/air-insulated-switchgear-market.
17. C. Ma, G. Moesch, B. Cabaret, and J. Tobias, *Innovative MV Switchgear for Today's Applications*. New York: IEEE, 2012, pp. 1–4. [CrossRef]
18. H. El Ouadhane, M. Haim, H. Spitzer, U. Kaltenborn, and R. Summer, "Solutions for internal arc protection acc.. iec 62271–200 with pressure relief into the switchgear room for gas and air insulated medium voltage switchgears," in Proc. of the 21st International Conference on Electricity Distribution, Frankfurt, Germany, 2011, pp. 1–5.
19. P. Kumar, A. Kale, A. K. Singh, and M. Ranade, "Internal arc fault simulation in medium voltage panel for thermal and structural withstand," in Proc. of the IEEE Holm Conference on Electrical Contacts. New York: IEEE, 2018, pp. 405–411. [CrossRef]
20. A. B. Wahle, and R. F. Summer, "Internal arc testing of medium voltage switchgear-Experiences with IEC 62271–200," in Proc. of the 19th International Conference on Electricity Distribution, Vienna, Austria, 2007.
21. R. P. P. Smeets, J.A.A.N. Hooijmans, N. Uzelac, P. Milovac, D. Kennedy, G.J. Pietsch and K. Anantavanich, "Internal arc testing of medium voltage switchgear," in Proc. of the 17th Conference on the Electric Power Supply Industry, (CEPSI), Macao, China, 2008.
22. D. Rochette, S. Clain, and F. Gentils, "Numerical investigations on the pressure wave absorption and the gas cooling interacting in A porous filter, during an internal arc fault in A medium-voltage cell," *IEEE Trans. Power Deliv.*, vol. 23, no. 1, pp. 203–212, 2007. [CrossRef]
23. N. Teera-Achariyakul, and J. Hokierti, "Internal arc pressure assessment of outdoor compact substation," in Proc. of the International Power Engineering Conference. New York: IEEE, 2005, pp. 1–70. [CrossRef]
24. S. Singh, D. S. Thevar, and O. Granhaug, "Internal arc root movement and Burnthrough prediction by simulation using first principle," Proc. of the 26th International Conference and Exhibition on Electricity Distribution, vol. 2021, No. 6, pp. 35–40, 2021. [CrossRef]
25. M. S. Ranade, A. Kale, and A. K. Singh, "A Three Dimensional CFD analysis to investigate the effect of ablative materials and venting arrangement on arc characteristics in low voltage circuit breakers," in Proc. of the IEEE 59th Holm Conference on Electrical Contacts. New York: IEEE, 2013, pp. 1–9. [CrossRef]
26. M. Matin, A. Dehghanian, M. Dastranj, and H. Darijani, "Explainable artificial intelligence modeling of internal arc in A medium voltage switchgear based on different CFD simulations," *Heliyon*, vol. 10, no. 8, e29594, 2024. [CrossRef]
27. E. Dullni, P. Wojcik, and T. Bleszynski, "Sentir la presión: Simulación del aumento de la presión en salas de Aparamenta," *Rev. ABB*, vol. 3, pp. 54–59, 2013.
28. V. Kumar, and S. Bhadri, "Life assessment of Micro-via used in thin Printed Circuit Board under Thermal Cycling loads & influence of selected design parameters," in Proc. of the IEEE 25th Electronics Packaging Technology Conference. New York: IEEE, 2023, pp. 710–715. [CrossRef]
29. A. Asplund, H. Remes, and Y. Ono, "Modeling of stress–strain fields below U-notch root using plasticity approximation rules under variable-amplitude loading," *Fatigue Fract. Eng. Mat. Struct.*, vol. 48, no. 2, pp. 900–913, 2025. [CrossRef]
30. C. Gong, T. Y. Niu, J. G. Gong, and F. Z. Xuan, "A time-dependent stress and strain estimation method for notched components under displacement-controlled condition," *Eng. Fract. Mech.*, vol. 242, p. 107447, 2021. [CrossRef]

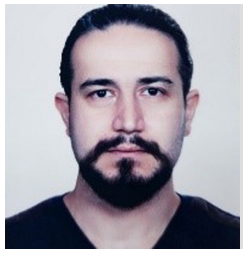

Ali Togay received his B.Sc degree in Mechanical Engineering from Kırıkkale University, Türkiye, in 2011. His M.Sc degree is ongoing in Energy Systems Engineering from Gazi University. His areas of interest are medium voltage switchgear, SF_6-Free systems, internal arc, power systems. He has been working in medium voltage sector for 13 years. He is currently an R&D Senior Engineer working at Eaton Corporation.

Gianmatteo Cantoro received his B.Sc degree in Mechanical Engineering, and his M.Sc and Ph.D degrees in Mechanical Engineering all from University of Bologna, in 2004,2006, and 2011, respectively. His areas of interest are plasma physics, plasma arc cutting torches, arc management and simulations. He is currently an R&D Lead Engineer working at Eaton Corporation.

Hıdır Düzkaya (IEEE M'17, SM'21) was born in Elazig, Turkey, in 1983. He received his B.Sc., M.Sc., and Ph.D. degrees in electrical engineering from Gazi University, Ankara, Turkey, in 2005, 2008, and 2019, respectively. He is currently with the Department of Electrical and Electronics Engineering, Gazi University, as a Research Assistant. He worked as a Post-Doctoral Researcher at the Ecole Centrale de Lyon, Écully, France, from 2020 to 2021. He has authored/co-authored more than 75 publications, including more than 30 refereed journal articles and three book chapters. His research focuses on high-voltage engineering, liquid dielectrics, gas-insulated systems, and gaseous dielectrics.

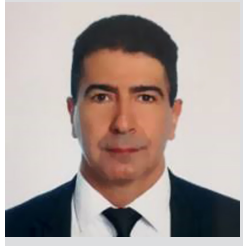

Müslüm Cengiz Taplamacıoğlu graduated from the Department of Electrical and Electronics Engineering, Gazi University, Ankara, Turkey. He received the M.Sc. degrees in Industrial Engineering from Gazi University and also in Electrical and Electronics Engineering from Middle East Technical University, Ankara, Turkey. He received his Ph.D. degree in Electrical, Electronics, and Systems Engineering from the University of Wales, Cardiff, UK. He is a Professor of Electrical and Electronics Engineering since 2000. He has authored/co-authored more than 150 publications, including more than 60 refereed journal articles and ten book chapters. His research interests and subjects are high voltage engineering, corona discharge and modelling, electrical field computation, measurement and modelling techniques, optical HV measurement techniques, power systems control and protection, lighting techniques, renewable energy systems, and smart grid applications.

Sabri Uzel received his B.Sc degree in Electirical Engineering from Istanbul Technical University, ITU, Türkiye at 2002. His areas of interest are medium voltage switchgear, SF_6-Free systems, high voltage, power systems. He has been working in medium voltage sector for 22 years. He is currently an R&D Electrical Manager working at Eaton Company.

Engin Göksu received his B.Sc degree in Mechanical Engineering from Eskişehir Osmangazi University, Türkiye, in 2010. His areas of interest are medium voltage switchgear, mechanism systems, SF_6-Free systems. He has been working in medium voltage sector for 15 years. He is currently an R&D Manager working at Eaton Corporation.

Tolga Ünver received his B.Sc and M.Sc degrees in Mechanical Engineering from Middle East Technical University, METU, Türkiye, in 1993 and 1998, respectively. His areas of interest are medium voltage switchgear, SF_6-Free systems, project management. He has been working in medium voltage switchgear sector for 8 years. He is currently an R&D Executive Manager working at Eaton Corporation.